

submitted to Phys. Rev. D
 preprint VAND-TH-99-12
Drafted on 1/11/2000

Signatures for a Cosmic Flux of Magnetic Monopoles

Stuart D. Wick¹, Thomas W. Kephart¹, Thomas J. Weiler¹
 and Peter L. Biermann²

¹ *Department of Physics & Astronomy, Vanderbilt University,
 Nashville, TN 37235*

² *Max Planck Institute for Radioastronomy,
 D-53010 Bonn, Germany*

Any early universe phase transition occurring after inflation has the potential to populate the universe with a flux of magnetic monopoles. Observations of galactic magnetic fields, and models for extragalactic magnetic fields, lead to the conclusion that monopoles of mass $\lesssim 10^{15}$ GeV are accelerated in these fields to relativistic velocities. We explore the possible signatures of a cosmic flux of relativistic monopoles impinging on the earth. The electromagnetically-induced signatures of monopoles are reliable. The hadronically-induced signatures are highly model-dependent. Among our findings are (i) the electromagnetic energy losses of monopoles continuously initiate a protracted shower of small intensity; (ii) monopoles may traverse the earth's diameter, making them a probe of the earth's interior structure; (iii) the best search strategy for monopoles is detection of their radio-Cherenkov signal produced by the coherent charge-excess in the $e^+ - e^-$ shower — in fact, underground radio-detectors have the potential to discover a monopole flux (or limit it) several orders of magnitude below the theoretical Parker limit of $10^{-15}/\text{cm}^2/\text{s}/\text{sr}$; (iv) it is conceivable (but not compelling) that bound states of colored monopoles may be the primary particles initiating the air showers observed above the GZK cutoff.

I. INTRODUCTION

Any breaking of a semisimple gauge symmetry which occurs after inflation and which leaves unbroken a $U(1)$ symmetry group may produce an observable abundance of magnetic monopoles. The initial monopole number density, and hence the present day flux of monopoles, can be estimated from the type and temperature of the symmetry breaking phase transition [1]. The monopole mass is expected to be $\sim \alpha^{-1}$ times the scale Λ_{SB} of the symmetry breaking. It is noteworthy that the inferred strength and coherence size of existing extragalactic magnetic fields

suggest that any monopole with a mass near or less than 10^{15} GeV would have been accelerated in magnetic fields to relativistic velocities. On striking matter, such as the earth's atmosphere, these relativistic monopoles will generate a particle cascade. It is the purpose of this paper to calculate the shower signatures of relativistic magnetic monopoles.

The electromagnetic interaction cross-section for relativistic monopoles is fairly well understood, but the hadronic cross-section is not. We calculate in some detail the reliable signatures resulting from the electromagnetic monopole-matter interaction. For the hadronic interactions of the monopole, we investigate various possibilities, and we present qualitative arguments for the resulting signatures.

On theoretical grounds, the monopole flux is limited only by Parker's upper bound $F_P \sim 10^{-15}/\text{cm}^2/\text{s}/\text{sr}$ [2], which results from requiring that monopoles not short-circuit our Galactic magnetic fields faster than their dynamo can regenerate them. The Parker bound is several orders of magnitude above the observed highest-energy cosmic ray flux. Thus, existing cosmic ray detectors can meaningfully search for a monopole flux, and proposed vast-area cosmic ray detectors may improve the search sensitivity by many orders of magnitude.

Because of the integrity of the monopole, the monopole primary will continuously induce an air-shower. This is in contrast to nucleon and photon primaries which transfer nearly all of their energy in the shower initiation. Thus we expect the monopole shower to be readily distinguished from non-monopole initiated showers. However, we also investigate the possibility that the hadronic interaction of the monopole is sufficiently strong to produce air-showers with dE/dx comparable to that from nuclear primaries, in which case existing data would already imply a meaningful limit on the monopole flux. One may even speculate that monopoles with a large dE/dx have been observed, as the primaries producing the enigmatic showers above the GZK cutoff at $\sim 5 \times 10^{19}$ eV [3,4].

The outline of this paper is as follows: In section (II) we discuss the limits on the monopole mass and number density. We examine the internal structure of monopoles and their natural kinetic energies from acceleration in large-scale cosmic magnetic fields. In section (III) expressions for the energy loss of relativistic monopoles are presented. The most reliable expressions incorporate the electromagnetic processes of ionization, electron pair production, and bremsstrahlung. The hadronic energy loss is also considered. In section (IV) we discuss signatures of relativistic monopoles arising from their electromagnetic energy loss processes. We develop a model for the electromagnetic particle shower induced by relativistic monopoles. Cherenkov signatures are examined, including the coherent radio-Cherenkov signal resulting from the shower charge excess. We mention the possible detection of the coherent Cherenkov signal in km^3 ice experiments. It is shown that monopoles may be sufficiently penetrating such that Earth tomography with relativistic monopoles is practicable. The detection of penetrating monopoles in the lunar regolith from their coherent radio-Cherenkov signal is also possible. The monopole's air fluorescence yield is found to be too low to allow the detection of monopoles in air showers, unless "baryonic-monopoles" could develop a "growing" strong cross-section. This possibility is explored in section (V) with a simplified model of the development of a growing strong cross-section. Finally, in section (VI) we give concluding remarks.

II. MONOPOLES AND MAGNETIC FIELDS

A. Monopole Mass and Number Density

As first shown by 't Hooft and Polyakov [5], the dynamical content and stability of magnetic monopoles in particle physics models is regulated by the patterns of symmetry breaking in these models. A classification is given in [7] based on homotopy theory. For illustration, we consider the simplest case of a semisimple gauge group G (i.e., G has no $U(1)$ factors) that breaks to a subgroup G' that is nonsemisimple (i.e., has at least one $U(1)$ factor which is part of a linear combination making up $U_{EM}(1)$). At the symmetry-breaking temperature $T_c \sim \langle \phi \rangle$ at which the order parameter $\langle \phi \rangle$ turns on, monopoles of mass $M \sim T_c/\alpha$ (α is the fine structure constant at scale T_c) appear. The order parameter can be the VEV of some scalar field or some bi-fermionic condensate that breaks the symmetry. We assume that the value of $\langle \phi \rangle$ is at or above the electroweak (EW) scale ~ 250 GeV so as to avoid violations of Standard Model (SM) physics. This assumption then bounds the monopole mass to be $\gtrsim 40$ TeV. We note that a similar lower mass bound results from (boldly) treating a classical monopole as a virtual quantum in radiative corrections to the SM [6].

The number density and therefore the flux of monopoles emerging from a phase transition are determined by the Kibble mechanism [1]. At the time of the phase transition, roughly one monopole or antimonopole is produced per correlated volume. The resulting monopole number density today is

$$n_M \sim 10^{-19} (T_c/10^{11} \text{ GeV})^3 (l_H/\xi_c)^3 \text{ cm}^{-3}, \quad (2.1)$$

where ξ_c is the phase transition correlation length, bounded from above by the horizon size l_H at the time when the system relaxes to the true broken-symmetry vacuum. The correlation length may be comparable to the horizon size (second order or weakly first order phase transition) or considerably smaller than the horizon size (strongly first order transition).

Phenomenologically, the monopole flux is constrained by cosmology and by astrophysics. Cosmology requires that the monopole energy density Ω_M not be so large as to add observable curvature to the universe. Astrophysics requires the monopole flux to respect the Parker bound such that the magnetic field of our galaxy is sustained. From Eq.(2.1) comes an expression for the monopole mass density today relative to the closure value

$$\Omega_M \sim 0.1 (M/10^{13} \text{ GeV})^4 (l_H/\xi_c)^3. \quad (2.2)$$

Monopoles less massive than $\sim 10^{13} (\xi_c/l_H)^{3/4}$ GeV do not overcurve the universe. Requiring that the Kibble flux in Eq. (2.4) be less than the Parker limit $F \equiv F_P \leq 10^{-15} \text{ cm}^2/\text{sec}/\text{sr}$, one derives a combined mass bound [4]

$$M \lesssim 10^{11} (\xi_c/l_H) \text{ GeV}. \quad (2.3)$$

This constraint is stronger than the curvature constraint by about two orders of magnitude.

In section (II C) we will show that free monopoles with $M \lesssim 10^{15}$ GeV are accelerated to relativistic energies by the cosmic magnetic fields.* From Eq.(2.1) then, the general expression for the relativistic monopole flux may be written [4]

* Due to the smallness of the monopole's Thomson cross-section for monopole masses of interest, $\sigma_T \sim 2 \times 10^{-43} (10^{10} \text{ GeV}/M)^2 \text{ cm}^2$, the mean free path for a monopole to scatter on the cosmic background radiation greatly exceeds the Hubble size of the universe [4].

$$F_M = c n_M / 4\pi \sim 2 \times 10^{-4} \left(\frac{M}{10^{15} \text{GeV}} \right)^3 \left(\frac{l_H}{\xi_c} \right)^3 \text{cm}^{-2} \text{sec}^{-1} \text{sr}^{-1}. \quad (2.4)$$

The energy-density constraint for relativistic monopoles is stronger than that for non-relativistic monopoles. From Eqs. (2.2) and (2.4) we may write for the *relativistic* monopole closure density [4]

$$\Omega_{RM} \sim \left(\frac{\langle E_M \rangle}{10^{28} \text{eV}} \right) \left(\frac{F_M}{F_P} \right). \quad (2.5)$$

This shows that a Kibble monopole flux respecting the Parker limit cannot overcurve the universe regardless of the nature of the monopole-creating phase transition (parameterized by ξ_c/l_H), as long as $\langle E_M \rangle \lesssim 10^{28} \text{eV}$.

Minimal $SU(5)$ breaking gives monopoles of mass $\sim 10^{17} \text{ GeV}$. However, within field theory there exist many possibilities to produce monopoles with mass below this scale. For example, there are other chiral $SU(N)$ [8] and chiral $O(N)$ models [9,10] with lighter monopoles. There are also relatively light monopoles ($M \sim 10^8 \text{ GeV}$) in the phenomenologically interesting $SU(15)$ model [11]. Recently, a new field theoretic possibility has emerged based on conformal field theory (CFT). This theory was discovered in the context of type IIB strings and M-theory compactifications on higher-dimensional anti-de Sitter space [12]. Nevertheless, the rules for constructing the 4D CFTs can be considered independently of any higher dimensional origins. These theories are naturally $N = 4$ supersymmetric, but, depending on the compactification, can have reduced $N = 0, 1, 2$, or 4 supersymmetry and a product of $SU(n_i)$ gauge groups. Three-family non-supersymmetric models have been constructed with GUT scale \sim few TeV [13]. Some of these models unify $U_{EM}(1)$ and $SU_C(3)$ [14] while others do not.

In yet another alternative, extra dimensions *a la* Kaluza-Klein [15,16] decrease M_{GUT} if these extra dimensions are not too tightly compactified. For example, with two extra dimensions of millimeter size, the GUT scale is lowered to about 100 TeV due to the dramatic change from logarithmic to power law running in the renormalization group equation. This low-scale unification in turn may lead to magnetic monopoles of mass $\sim 10^4 \text{ TeV}$. A potential concern for monopoles in higher-dimensional theories is topological instability, i.e. monopoles in greater than four dimensions may unwind. However, monopoles made of SM fields confined to the three-dimensional brane would remain stable. In fact, there are even richer possibilities for monopoles in higher-dimensional theories. New defect solutions may exist in the larger dimensions, stabilized by topology. The intersection of these new solutions on the SM brane could then be monopoles, stabilized by the usual 3D topological argument.

A relatively low GUT scale seems to be necessary to allow light-mass monopoles. It should be remarked that a low GUT scale will typically also enable fast proton decay, in violation of experimental lifetime bounds. However, some of the 4D field theory models listed above have accidental symmetries (continuous or discrete) which stabilize the proton. The $SU(15)$ model has no direct gauge induced proton decay and the proton decay in the MSSM Pati-Salam Model [8] is only induced through the hidden sector. The higher dimensional models have additional stabilizing possibilities.

To summarize this section, there are ample theoretical possibilities for producing monopoles with mass $\lesssim 10^{15} \text{ GeV}$ and the possibility of strong interaction cross-sections that avoid proton decay. Based on the Kibble mechanism for monopole production, bounds on the universe's curvature constrain the monopole mass to less than 10^{13} GeV , while a comparison of the Kibble flux to the Parker limit constrains the monopole mass to less than 10^{11} GeV . However, we note that in higher dimensional cosmologies the Kibble flux given in eq. (2.4) may be altered. If the Kibble flux estimate is changed, then the straightforward Parker upper limit $F_P \leq 10^{-15} / \text{cm}^2 / \text{sec} / \text{sr}$ becomes the only reliable bound on the monopole flux. Thus, in the spirit of generality, we will let M be a free parameter and use the Kibble

mechanism as a rough guide to F_M . We will, of course, require that F_M obey the Parker limit. We also will assume that proton decay is avoided in a way that does not restrict the parameter M .

B. Monopole Structure

The fact that monopoles are topological defects endows them with a non-trivial internal structure; the core of the monopole is a region of restored unified symmetry. Monopoles are classified [1] by their topological winding, but for the case of GUT monopoles this classification is coarse. A finer classification [17,18] shows a spectrum of GUT monopoles consisting of six different fundamental monopoles. Classical bound states of the fundamental monopoles have been studied for the case of unification into minimal $SU(5)$. Remarkably, the spectrum of bound-state monopoles corresponds almost exactly to the particle spectrum of one standard model family.

In this work we need to distinguish between those monopoles with color-magnetic charge and those with only ordinary ($U_{EM}(1)$) magnetic charge. Thus, we adopt the nomenclature “ q -monopoles” for those monopoles with color-magnetic charge and “ l -monopoles” for those with only the ordinary magnetic charge.

The similarity of the GUT monopole spectrum with the standard model particle content has been recognized and an attempt to construct a “dual standard model” [18] out of monopoles has been undertaken. In another approach to the study of GUT monopoles, their possible confinement has recently been considered [19] via the formation of Z_3 color-magnetic “strings.” If such a mechanism was realized one result could be the formation of color-singlet “baryonic-monopoles.” In this picture the fusion of three differently colored strings produces a baryon-like composite of fundamental GUT monopoles.

The internal structure of a baryonic-monopole would approximate that of an ordinary baryon in the QCD string model, but with q -monopoles in the place of quarks. Thus, the baryonic-monopole structure is quite different from a single l -monopole and as such we expect it to have a very different hadronic cross-section and, therefore, cosmic ray shower profile. Throughout this paper we entertain the notion that q -monopoles would have formed baryonic-monopoles which then comprise a significant fraction of the relic monopole density. In sec. (V) we mention the viability of baryonic-monopoles as candidate primaries for the super-GZK airshowers.

C. Monopole Acceleration

The kinetic energy imparted to a magnetic monopole on traversing a magnetic field is [4]

$$E_K = gB \int_{\mathcal{C}} \vec{\xi} \cdot \hat{dv}, \quad (2.6)$$

where

$$g = e/2\alpha = 3.3 \times 10^{-8} \text{ esu} \quad (\text{or } 3.3 \times 10^{-8} \text{ dynes/G}) \quad (2.7)$$

is the Dirac magnetic charge, B is the magnetic field strength, $\vec{\xi}$ specifies the field’s coherence length and direction, \mathcal{C} is the curve describing the monopole path, and \hat{dv} is the direction of the monopole velocity at a given point along the path. In Table 1 we indicate the cosmic magnetic fields and their coherence lengths, inferred from observations of

synchrotron radiation and Faraday rotation, and from modeling. The typical values of the monopole kinetic energies that result from these fields are also shown in the Table. A similar table has been constructed by [20]. The largest energies are seen to come from the magnetic fields having the longest coherence lengths. The strength of these sheet fields is inferred from simulations [21] and observations [22].

We emphasize that a typical monopole which travels through the universe, and has a mass below the energies indicated in Table 1, should be relativistic. Monopoles will gain and lose energy as they random-walk through the universe, eventually producing a broad distribution of energies (with $\Delta E_K/E_K \sim 1$) centered roughly on \sqrt{n} times the typical energy for a single transit through a region of homogeneous magnetic field. Here, n is the number of coherent fields encountered in the random walk. For extragalactic sheets, which we expect to dominate the spectrum, this number can be roughly estimated to be of order $n \sim H_0^{-1}/50 \text{ Mpc} \sim 100$, and so $E_{\text{max}} \sim 10^{25} \text{ eV}$. Hence, monopoles with mass below $\sim 10^{15} \text{ GeV}$ are relativistic.

It is anticipated that in the near future more reliable inferences of the extra-galactic magnetic fields will become available [24,27]; then the monopole energies and signatures we derive here can be made firmer. As a prelude to calculating monopole signatures in various detectors, we discuss the interactions of monopoles with matter in the next section.

	$B/\mu\text{G}$	ξ/Mpc	$gB\xi/\text{eV}$	Refs.
normal galaxies	3 to 10	10^{-2}	$(0.3 \text{ to } 1) \times 10^{21}$	[23]
starburst galaxies	10 to 50	10^{-3}	$(1.7 \text{ to } 8) \times 10^{20}$	[24]
AGN jets	~ 100	$10^{-4} \text{ to } 10^{-2}$	$1.7 \times (10^{20} \text{ to } 10^{22})$	[25]
galaxy clusters	2 to 30	$10^{-4} \text{ to } 1$	$3 \times 10^{18} \text{ to } 5 \times 10^{23}$	[26]
Extragal. sheets	0.1 to 1.0	1 to 30	$1.7 \times 10^{22} \text{ to } 5 \times 10^{23}$	[21]

TABLE I. Estimated magnetic field strength and coherence length for some astrophysical environments, and the associated monopole energies for a single transit through the regions.

III. RELATIVISTIC MONOPOLE ENERGY LOSS IN MATTER

GUT monopoles are formed in non-trivial representations of $SU_C(3) \times SU_L(2) \times U_Y(1)$ and couple to the standard model gauge fields. An accurate description of the monopole stopping power must include all of the standard model interactions or the relevant subset of those interactions for the type of monopole considered. In this paper we choose to ignore the weak interaction throughout, which is suppressed by factors $\sim M_Z^{-2}$. The electromagnetic and strong interactions will be accounted for in this section.

Regardless of the interaction, the fact that the massive monopole is conserved in each interaction, due to its topological stability, argues for kinematics rather different from those applying to nucleon or photon primaries. The differing kinematics in turn argues for differing signatures. However, our explorations of possible strong interactions will include a model where q -monopoles are excited and their hadronic cross-section grows after impact, so that the energy transfer is large enough to stop the monopole very quickly. In this model, the monopole's hadronic signature may be similar to that from a nucleon.

The strong interaction of a monopole is difficult to assess. Color confinement ensures that all monopoles are color singlet objects, and so have no classical long-range color-magnetic field. However, we expect l -monopoles and q -monopoles to have very different hadronic interactions. Although l -monopoles lack a color-magnetic charge, the unbroken symmetry in their core ensures that gluon and light quark fields will leak out from the center to the confinement distance $\Lambda_{QCD}^{-1} \sim \text{fm}$.

We will resume the discussion of the monopole's hadronic interaction with matter after first discussing in some detail their better-understood electromagnetic interactions. The electromagnetic interaction of the monopole may dominate the hadronic interaction because the electromagnetic coupling of the monopole is large,

$$\alpha_M = g^2 = \frac{1}{4\alpha} \simeq 34, \quad (3.1)$$

and mediated by a long-range field. At large distances and high velocities, the magnetic monopole mimics the electromagnetic interaction of a heavy ion of charge $Z \sim \frac{1}{2\alpha} \simeq 68$. We will follow others and treat the electromagnetic interaction of the monopole with matter semi-classically, i.e., viewing the monopole as a classical source of radiation, while treating the matter-radiation interaction quantum-mechanically. In this way, the large electromagnetic coupling of the monopole is isolated in the classical field, and the matter-radiation interaction can be calculated perturbatively.[†]

A. Electromagnetic Interactions

We consider here the energy losses of the monopole due to the three electromagnetic processes: collisions (ionization of atoms), e^+e^- pair production, and bremsstrahlung. It will turn out that Bethe-Heitler pair production will be the dominant mechanism for the growth of the total shower electron number N_e , which in turn is the source generating the Cherenkov and radio wave signatures. On the other hand, the bremsstrahlung process will be the major energy loss mechanism and so is the main contributor to the nitrogen fluorescence signature.

[†] Recent progress in quantizing the interacting monopole can be found in [28].

Three different γ -factors will be relevant in the energy-loss formulae. They are the boost factor of the monopole in the lab frame,

$$\gamma_{\text{lab}}^M = \frac{E_M}{M}, \quad (3.2)$$

the boost factor of the monopole in the center of momentum (cm) frame,

$$\gamma_{\text{cm}}^M = \frac{1 + \frac{\gamma_{\text{lab}}^M m_N}{M}}{\sqrt{1 + \frac{2\gamma_{\text{lab}}^M m_N}{M}}}, \quad (3.3)$$

and the target nuclei's boost factor in the cm-frame

$$\gamma_{\text{cm}}^N = \frac{\gamma_{\text{lab}}^M}{\sqrt{1 + \frac{2\gamma_{\text{lab}}^M m_N}{M}}}. \quad (3.4)$$

γ_{cm}^N is also the boost factor between the lab and the cm, because the nuclei are at rest in the lab frame. For this reason, we will use the simpler notation $\gamma_{\text{cm}} \equiv \gamma_{\text{cm}}^N$. In addition, the factor γ_{lab}^M occurs sufficiently frequently that we will drop the indices and simply rename it $\gamma \equiv \gamma_{\text{lab}}^M$.

Two useful limits for γ_{cm} are (i)

$$\gamma_{\text{cm}} \simeq \sqrt{\frac{\gamma M}{2Am_p}} \quad \text{for } \gamma \gg \frac{M}{2m_N}; \quad (3.5)$$

and (ii)

$$\gamma_{\text{cm}} \simeq \gamma \quad \text{for } \gamma \lesssim \frac{M}{2m_N}; \quad (3.6)$$

where A is the nuclear atomic number and $m_N = Am_p$, is the nuclear mass.

The monopole-matter electromagnetic interaction for $\gamma < 100$ is well reported in the literature [29,30]. Previous works include atomic excitations and ionization losses with electrons in the absorber. The density suppression effect is also included. In the literature these effects are collectively referred to as “collisional” energy losses and we follow that nomenclature here.

For $\gamma > 100$ the expression for collisional energy losses needs to be modified, and QED effects like primary particle bremsstrahlung and electron-positron pair production can become operative. As we are interested in the energy loss of ultrarelativistic monopoles in matter, we will need to consider these processes.

1. Collisional Energy Loss

The magnetic monopole stopping power formula calculated by Ahlen [30] includes ionization of the absorber at small impact parameters and atomic excitation at large impact parameters. For highly relativistic monopoles we ignore the various correction terms and simply describe ionization with

$$\frac{dE_{\text{coll}}}{dx} = -\frac{\pi N_e}{m_e} \left[\ln \left(\frac{m_e \beta^2 \gamma^2}{I} \right) - \frac{\delta}{2} \right]. \quad (3.7)$$

In eq. (3.7) N_e is the electron number density of the absorber, m_e is the electron mass, I is the mean ionization energy of the medium, and δ is the density effect [31].

2. Bethe-Heitler Process

For a relativistic monopole primary the electron-positron pair production cross section [32,33] gives a stopping-power [30,34]

$$\frac{dE_{\text{pair}}}{dx} \simeq -\frac{16}{3 \times 10^3} \frac{g^2 e^2 Z \alpha N_e}{m_e} \gamma_{\text{cm}} \ln(\gamma), \quad (3.8)$$

where Z is the atomic number of the atoms comprising the absorber. Based on dynamical arguments [35] the electron-positron pair is produced roughly at rest in the center of mass frame. For large M , the produced pair will be nearly at rest with respect to the monopole and so the final expression for the pair production stopping power is

$$\frac{dE_{\text{pair}}}{dx} \simeq -\frac{1}{10^5} \frac{ZN_e}{m_e} \frac{\gamma}{\sqrt{1 + \frac{2\gamma Am_p}{M}}} \ln(\gamma). \quad (3.9)$$

The Bethe-Heitler process dominates collisional energy loss at high velocities, when the density effect [31] suppresses ionization. For highly relativistic monopoles ($\gamma > 1000$) the collisional energy loss can be ignored.

3. Monopole Bremsstrahlung

The energy radiated in a relativistic collision is proportional to the incident charged particle's acceleration, i.e., inversely proportional to its mass, so we expect bremsstrahlung to be negligible for the larger massed monopoles. For the lightest allowed monopoles, however, bremsstrahlung will contribute and in fact can dominate the energy loss because of the strong monopole coupling to the photon field.

The approximate stopping power with negligible nuclear screening[‡] has been calculated [36] and for monopoles [34] will be

$$\frac{dE_{\text{rad}}}{dx} \simeq -\frac{16}{3} \frac{ZN_e \alpha \alpha_M^2}{M} \gamma \ln \gamma \simeq -\frac{137}{3} \frac{ZN_e}{M} \gamma \ln \gamma. \quad (3.11)$$

Bremsstrahlung will dominate the Bethe-Heitler process for boost factors

$$\gamma \gtrsim \frac{10^5}{A} \left(\frac{M}{100 \text{ TeV}} \right)^3. \quad (3.12)$$

Integrating eq. (3.11) gives

$$\gamma(x) = \gamma_0^{\exp(-\kappa x)} \quad (3.13)$$

where

[‡] Screening of the nuclear charge by the atomic electrons is large when [36,34]

$$\gamma > \frac{192M}{m_e Z^{\frac{1}{3}}} \simeq \frac{3 \times 10^{10}}{Z^{\frac{1}{3}}} \left(\frac{M}{100 \text{ TeV}} \right). \quad (3.10)$$

Thus, even for the lightest monopoles which we consider, eq. (3.10) shows that screening corrections are expected to be small.

$$\kappa \equiv \frac{137}{3} \frac{ZN_e}{M^2} = 10^{-11} \frac{\text{cm}^2}{\text{g}} \left(\frac{Z}{10} \right) \left(\frac{N_e}{N_A/\text{cm}^3} \right) \left(\frac{100\text{TeV}}{M} \right)^2, \quad (3.14)$$

where N_A is Avagadro's number. For $\kappa x \ll 1$, which holds for monopoles at earth, we may use the approximation $\exp(-\kappa x) \sim 1 - \kappa x$, which gives

$$\gamma(x) \simeq \gamma_0^{1-\kappa x}. \quad (3.15)$$

Thus, the characteristic length-scale for attenuating the monopole kinetic energy via bremsstrahlung is κ^{-1} .

B. Hadronic Interactions

As previously mentioned, all GUT monopoles contain internal color fields. The l -monopole's color field is soft, extending to a distance $\Lambda_{QCD}^{-1} \sim \text{fm}$. In this regard, its internal color is similar to that of a normal hadron. However, there are no valence quarks internally, and so a better analogy to the color structure of an l -monopole is a glueball. Thus, we expect the hadronic cross-section of l -monopoles to be of typical hadronic strength, with a fractional energy transfer of order $\Delta E/E \sim \Lambda_{QCD}/M \sim 10^{-10} (10^{10}\text{GeV}/M)$. For l -monopoles an approximate hadronic stopping power would then be

$$\frac{dE_{\text{had}}}{dx} \simeq -\frac{\gamma \Lambda_{QCD}}{\lambda} \simeq -\gamma \Lambda_{QCD} N_n \sigma_{\text{had}} \quad (3.16)$$

where the mean-free-path between hadronic interactions is $\lambda = (N_n \sigma_{\text{had}})^{-1}$, for a nucleon density N_n and a typical hadronic cross-section σ_{had} . Generally, the electromagnetic interaction will dominate the hadronic interaction for l -monopoles.

The q -monopoles are quite different. Inside each baryonic-monopole, three constituent q -monopoles are confined by strings of Z_3 color-magnetic flux into a color-singlet. Although the baryonic-monopoles offer a large mass-scale realization of the QCD string model, the scattering of these monopoles will behave very differently from typical hadrons. Whereas quark-antiquark pairs are readily produced when a color-electric string stretches and breaks, the color-magnetic string may only be broken with the production of a monopole-antimonopole pair. Monopole pair production is highly suppressed for two reasons, the large monopole mass-scale and the fact that monopoles are composite objects. The QCD string model, with total cross-section growing with string length, may serve as a guide in understanding baryonic-monopole hadronic interactions with the significant caveat that the confining strings in the monopole are readily stretched but not broken. The energy loss for baryonic-monopoles can be approximated as

$$\frac{dE_{\text{had}}}{dx}(x) \simeq -\frac{\gamma \Lambda_{QCD}}{\lambda(x)} \simeq -\gamma \Lambda_{QCD} N_n \sigma_{\text{had}}(x), \quad (3.17)$$

where the strong cross-section is explicitly a function of column depth. We defer further discussion of these extended strong interactions until section (V), to allow us to focus first on the signatures that result from the better-understood electromagnetic interaction.

IV. MONOPOLE ELECTROMAGNETIC SIGNATURES

Signature events for l -monopoles are derived below with a specific emphasis on 1) the general shower development, 2) Cherenkov signatures, 3) Earth tomography with relativistic l -monopoles, and 4) the nitrogen fluorescence signature. The general shower characteristics are developed first as the other signatures are derivable from that model.

A. Monopole Shower Development

The l -monopoles will be highly penetrating primaries, interacting mostly via the electromagnetic force and all the while maintaining their structural integrity. On average, there will be a quasi-steady cloud of secondary particles traveling along with the l -monopole. Thus, we will call this type of shower “monopole–induced.” For the remainder of sec. (IV) we only consider l -monopoles to which we will simply refer to as “monopoles”.

1. Monopole–Induced Subshowers

Given a fast monopole passing through matter, the various electromagnetic processes discussed in sec. (III) can inject energetic photons, electrons, and positrons into the absorbing medium. If the energy of these injected secondary particles is sufficient, they may initiate a particle cascade. We now give a review of a simple model to describe such a cascade.

An electromagnetic cascade can be initiated by an electron, positron or photon. In the simple model we consider, the photon pair production length is equal to the electron (or positron) radiation length. In this model, originally developed by Heitler [37] and reviewed in [38,39], photon and electron showers will develop identically. Consider a photon primary of initial energy E_0 which travels a distance R through the absorber before pair producing.[§] The two particles in the produced pair are then assumed to share equally the initial photon’s energy, i.e., they each receive an energy $\frac{E_0}{2}$. After traveling another distance R the electron and positron each radiate a bremsstrahlung photon where the produced photon takes half the parent energy. The particle number has doubled again and the energy per particle is halved again so that the 4 particles at this stage each have an energy $\frac{E_0}{4}$. The shower continues to develop in this exponential fashion until the energy per particle drops to where particle production is no longer the dominant energy loss process. This is the critical energy, E_c , below which ionization of the absorber dominates the energy loss processes. For typical materials, $E_c \simeq 100$ MeV.

R is evidently the distance over which the energetic particle will lose $\frac{1}{2}$ its energy and is therefore related to the radiation length**, ξ_e , by $R = \xi_e \ln 2$. This relation is apparent from

[§]The particle doubling length, R , can be lengthened significantly by the Landau-Pomeranchuk-Migdal effect [40,41] for photon or electron energies $E \gtrsim E_{\text{LPM}}$. The value of E_{LPM} is dependent on the material and some typical values are $E_{\text{LPM}} = 2.2$ TeV for lead, $E_{\text{LPM}} = 139$ TeV for water, and $E_{\text{LPM}} = 117$ PeV for sea level air [40]. This model assumes that $E \ll E_{\text{LPM}}$ which is generally the case for e^\pm and γ originating from monopole–nucleus interactions.

**Recall that the radiation length is given by $\frac{dE}{dx} = -\frac{E}{\xi}$, so that the energetic particle will lose e^{-1} of its energy per radiation

$$E(x) = E_0 2^{-\frac{x}{R}} = E_0 e^{-\frac{x}{\xi_e}}. \quad (4.1)$$

After the shower develops through a distance nR there will be 2^n particles in the shower. In the continuum approximation the number of particles comprising the shower at a given depth is

$$N(x) = 2^{\frac{x}{R}} = e^{\frac{x}{\xi_e}} \quad (4.2)$$

and the maximum number produced must be $N_{\max} = \frac{E_0}{E_c}$. The depth of the shower maximum, X_{\max} , can be derived from the relation

$$\frac{E_0}{E_c} = N_{\max} = 2^{\frac{X_{\max}}{R}} = e^{\frac{X_{\max}}{\xi_e}} \quad (4.3)$$

which gives

$$X_{\max} = \frac{\ln\left(\frac{E_0}{E_c}\right)}{\ln 2} R = \xi_e \ln\left(\frac{E_0}{E_c}\right). \quad (4.4)$$

The value of ξ_e in air is quoted as 34 g/cm^2 [39], while the value in ice is quoted as 36 g/cm^2 [51]. As the two values are very similar, we will use in our numerical work the average value 35 g/cm^2 .

After reaching the shower maximum at X_{\max} the shower size decreases exponentially with column depth. The attenuation length for the shower decay after X_{\max} is approximately $200 \frac{\text{g}}{\text{cm}^2}$ [42].

2. Longitudinal Shower Profile

A monopole is highly penetrating and, as such, can initiate many cascades before stopping, but the energy injected into the absorber in any single interaction must be greater than E_c for a subshower to develop. This restricts the inelasticity to $\eta \gtrsim \frac{E_c}{E_0} \simeq 10^{-12} \left(\frac{E_0}{10^{20} \text{ eV}}\right)^{-1}$, for monopole-matter interactions which can develop subshowers and contribute to the quasi-steady cloud of secondary particles traveling with the monopole. Lower inelasticity events will contribute directly to ionization without intermediate particle production.

Suppose the monopole initiates the j^{th} subshower at a depth x_j . The subsequent development of the j -subshower is

$$N_j(x) = N_0 e^{\frac{(x-x_j)}{\xi_e}} \quad (4.5)$$

where $0 < (x - x_j) < \xi_e \ln\left(\frac{E_j}{N_0 E_c}\right)$, the total energy injected into the shower at the point x_j is E_j , and N_0 is the initial number of particles injected into the shower at the point x_j . (For electron pair production $N_0 = 2$, whereas for bremsstrahlung and monopole-electron elastic scattering $N_0 = 1$.)

The total shower development $N(x)$ is then obtained by summing over all the subshowers

$$N(x) = \sum_j N_j(x). \quad (4.6)$$

length.

The approximate distance between the initiation of subshowers is given by the mean free path, $\lambda = \frac{1}{\sigma n}$, where σ is the cross section for the relevant process and n is the number density of scattering centers. The j^{th} interaction then will roughly occur at the depth $x_j = j\lambda$. If the inelasticity per interaction is approximately given by a constant value of η then the energy injected at the j^{th} scattering is

$$E_j = \frac{\eta}{1-\eta} (1-\eta)^j E_0. \quad (4.7)$$

The sum in eq. (4.6) can now be performed from $j = 1$ to the integer nearest $\frac{x}{\lambda}$ and where the condition $0 < (x - x_j) < \xi_e \ln \left(\frac{E_j}{N_0 E_c} \right)$ must remain satisfied.

The monopole will continue to initiate subshowers until it is degraded in energy to the point where $E_j \simeq N_0 E_c$. That fixes the maximum number of subshowers to be

$$j_{\max} = \frac{\ln \left(\frac{(1-\eta)N_0 E_c}{\eta E_0} \right)}{\ln(1-\eta)}. \quad (4.8)$$

The sum in eq. (4.6) can be transformed into an integral over column depth by making a continuum approximation. The substitution $\sum_j \rightarrow \int \frac{dx_j}{\lambda}$ and taking $x_j \rightarrow x'$ gives

$$N(x) = \int_{x_{\min}}^x \frac{dx'}{\lambda} e^{\frac{(x-x')}{\xi_e}} = \frac{\xi_e}{\lambda} \left[e^{\frac{(x-x_{\min})}{\xi_e}} - 1 \right]. \quad (4.9)$$

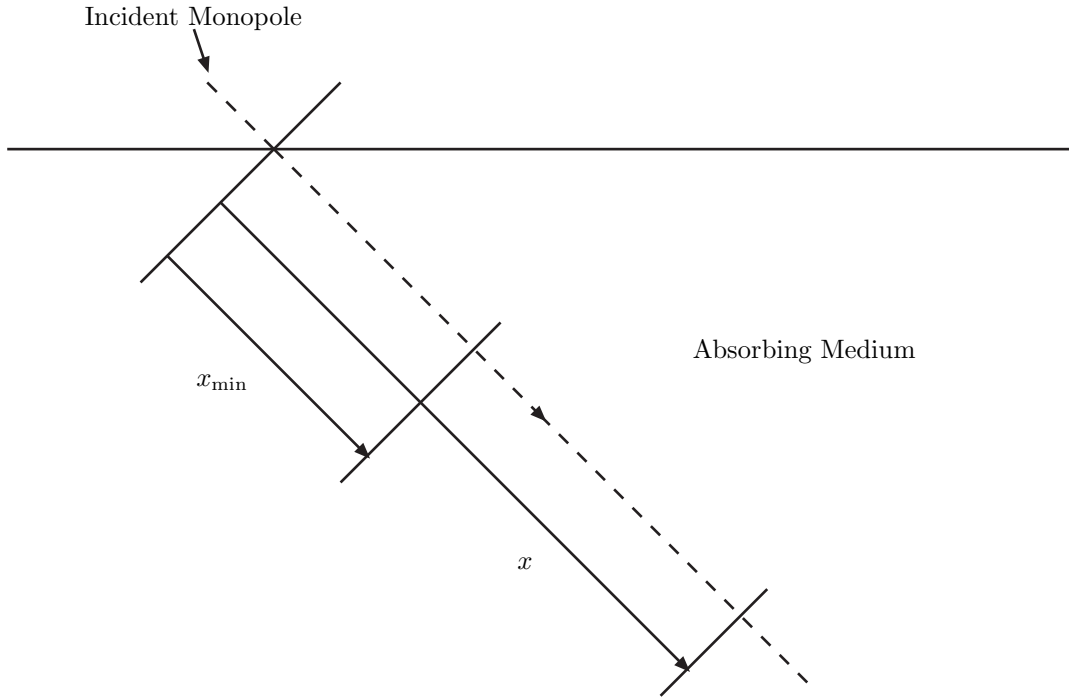


FIG. 1. A schematic representation of the variables entering into a calculation of the shower development for a monopole-induced shower. The monopole path is along the dashed line. The depth where the shower size is evaluated is at x . The smallest depth where an initiated subshower contributes to the total shower is at x_{\min} .

The physical interpretation of the limits of integration is as follows (also see fig. (1)): x_{\min} is the smallest depth at which an initiated subshower is still cascading at the depth x . Subshowers initiated at depths $< x_{\min}$ will have already ranged out by the point x ,^{††} so they cannot contribute to the particle number at x and are excluded from the integral.

From the geometry of fig. (1), using eq. (4.4), and taking $j \rightarrow \frac{x}{\lambda}$ we can deduce

$$x_{\min}(x) = x - X_{\max}^j = x - \xi_e \ln \left(\frac{\eta(1-\eta)^{\frac{x_{\min}}{\lambda}} E_0}{(1-\eta) N_0 E_c} \right). \quad (4.10)$$

Solving for x_{\min} gives

$$x_{\min} = \frac{x - \xi_e \ln \left(\frac{\eta E_0}{(1-\eta) N_0 E_c} \right)}{1 + \frac{\xi_e}{\lambda} \ln(1-\eta)}. \quad (4.11)$$

Using $\eta \ll 1$, so $\ln(1-\eta) \simeq -\eta$ and $\frac{\eta}{1-\eta} \simeq \eta$, simplifies this to

$$x_{\min} = \frac{x - \xi_e \ln \left(\frac{\eta E_0}{N_0 E_c} \right)}{1 - \frac{\eta \xi_e}{\lambda}}. \quad (4.12)$$

Considering that $0 < \eta < 1$, this expression could be singular, but we will see that for monopoles this is not a concern.

A useful relation between the continuum and discrete expressions for energy loss is

$$\frac{\eta E}{\lambda} = \left| \frac{dE}{dx} \right|. \quad (4.13)$$

From eq. (3.11) $\frac{1}{E} \left| \frac{dE}{dx} \right| = \kappa \ln(\gamma)$, so the eq. (4.12) can be written

$$x_{\min} = \frac{x - X_{\max}^0(\eta)}{1 - \xi_e \kappa \ln(\gamma)}. \quad (4.14)$$

For the remainder of this section we define $X \equiv X_{\max}^0(\eta) = \xi_e \ln \left(\frac{\eta E_0}{N_0 E_c} \right)$, which is the depth of the subshower maximum when the monopole has its full kinetic energy, E_0 .

For a monopole passing through normal matter $\xi_e \kappa \ln(\gamma) \ll 1$, so we can write eq. (4.14) as

$$x - x_{\min} = X + (X - x) \xi_e \kappa \ln(\gamma). \quad (4.15)$$

Substituting the above into eq. (4.9) gives

$$N(x, \gamma) = \frac{\xi_e}{\lambda} \left[\exp \left(\frac{X}{\xi_e} \right) \gamma^{\kappa(X-x)} - 1 \right]. \quad (4.16)$$

Using the relationship of eq. (4.13)

$$N(x, \gamma) = \xi_e \left| \frac{dE}{dx} \right| \left[\frac{\gamma^{\kappa(X-x)}}{N_0 E_c} - \frac{1}{\eta E(x)} \right] \quad (4.17)$$

^{††} We neglect particles after their energies fall below E_c . Omission of this exponentially-decaying tail results in an underestimate of the true particle number by a factor of order a few. This makes a negligible difference as far as the coherent-shower Cherenkov emission is concerned. It makes some difference to the longitudinal profile, and therefore to the fluorescence signal. However, we show in section IV D that the fluorescence signal from a monopole is weak, probably too weak to be measured.

where $N(x, \gamma)$ must be non-negative by definition.

At this point, we need to consider which processes will contribute most to the function $N(x, \gamma)$. The fact that $N(x, \gamma)$ is $\propto \frac{dE}{dx}$, which is dominated by bremsstrahlung and pair production at large γ , means that we can ignore the small collisional losses. Furthermore, the bremsstrahlung process is generally too soft ($E_\gamma < E_c$) to contribute significantly to the growth of $N(x, \gamma)$. That leaves pair production as the main contributor to eq. (4.17). For pair production, $N_0 = 2$ and $\eta E(x) \simeq 2\gamma_{\text{cm}} m_e$. Assuming $E_c \simeq 100$ MeV, the term in square brackets is positive where $\gamma \gtrsim 200$.

Finally, the longitudinal shower distribution is

$$N(x, \gamma) \simeq \frac{10^{-5} \xi_e Z N_e}{2E_c m_e} \frac{\ln(\gamma) \gamma^{1+\kappa(X-x)}}{\sqrt{1 + \frac{2\gamma A m_p}{M}}} \left[\frac{1}{N_0 E_c} \gamma^{\kappa(X-x)} \right]. \quad (4.18)$$

A parameterization of ξ_e in different media, good to $\lesssim 2.5\%$, is given by [43]

$$\xi_e = \frac{716.4 \frac{\text{g}}{\text{cm}^2} A}{Z(Z+1) \ln\left(\frac{287}{\sqrt{Z}}\right)} \quad (4.19)$$

and a fit to the data [44] for E_c is

$$E_c = \begin{cases} \frac{610 \text{ MeV}}{Z+1.24} & \text{for solids and liquids} \\ \frac{710 \text{ MeV}}{Z+0.92} & \text{for gases} \end{cases}. \quad (4.20)$$

It is surprising, and may seem counter-intuitive, that the shower profile changes very little while the monopole passes through a medium boundary. For example, in traveling from mantle into air the shower size is reduced by $\sim 30\%$ while the density decreases by $\sim 10^{-4}$. In a more dense medium there are more interactions per unit path-length but the subshowers range out more quickly. Thus, the monopole-induced quasi-steady shower is mostly fixed by the properties of the monopole and only weakly determined by the absorber medium. The shower size over the full range $200 < \gamma < 10^{10}$ is given by eq. (4.18). We plot this function for the different terrestrial media in figures 2, 3, and 4 for $x \ll \kappa^{-1}$. As can be gleaned by comparing these three figures, the shower size is almost independent of the medium.

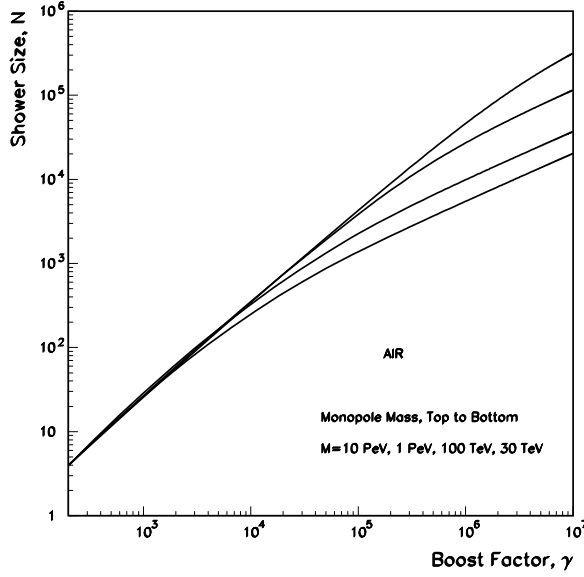


FIG. 2. The monopole-induced quasi-steady shower size in air, for monopoles in the mass range $30\text{TeV} < M < 10\text{PeV}$. The shower size is the total number of electron, positrons, and photons.

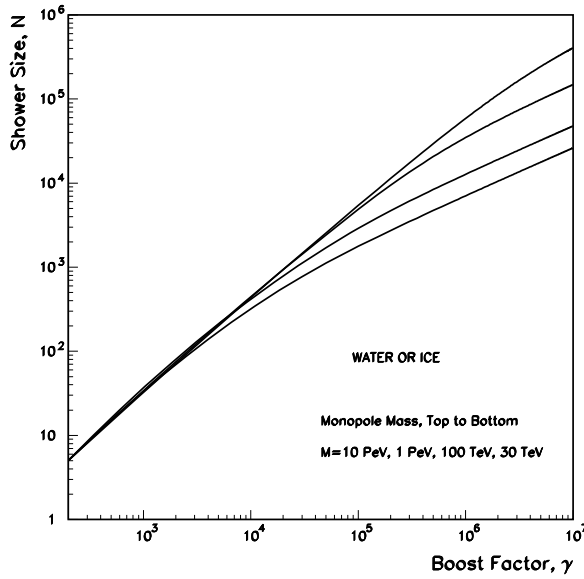


FIG. 3. The monopole-induced quasi-steady shower size in water (or ice), for monopoles in the mass range $30\text{TeV} < M < 10\text{PeV}$. The shower size is the total number of electron, positrons, and photons.

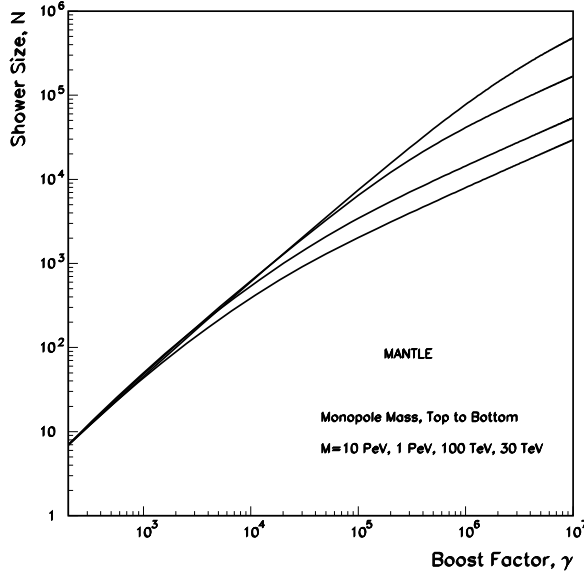


FIG. 4. The monopole-induced quasi-steady shower size in the earth's mantle for monopoles in the mass range $30\text{TeV} < M < 10\text{PeV}$. The shower size is the total number of electron, positrons, and photons.

3. Lateral electromagnetic profile

For monopole-induced showers the lateral profile is greatly simplified in comparison to hadronic primaries. As shown previously, the monopole-induced shower size is approximately constant because it is continuously being regenerated as the lower energy particles range out. For our purposes in the following section it is sufficient to assume that the lateral profile is uniform out to a lateral cutoff given by the Molière radius

$$R_M = 7.4 \left(\frac{\xi_e}{35\text{g/cm}^2} \right) \left(\frac{100\text{MeV}}{E_c} \right). \quad (4.21)$$

As defined, the Molière radius is independent of the incident monopole energy, being determined only by the spread of low energy particles resulting from multiple Coulomb scattering. Within a distance R_M of the monopole path will be $\sim 90\%$ of the shower particles. [43]

B. Monopole Cherenkov Signatures

When a charge travels through a medium with index of refraction n , at a velocity $\beta > \frac{1}{n}$, Cherenkov radiation is emitted [45]. The total power emitted in Cherenkov radiation per unit frequency ν and per unit length l by a charge Ze is given by the Frank-Tamm formula

$$\frac{d^2W}{d\nu dl} = \pi\alpha Z^2 \nu \left[1 - \frac{1}{\beta^2 n^2} \right]. \quad (4.22)$$

The maximal emission of the Cherenkov light occurs at an angle

$$\theta_{\max} = \arccos\left(\frac{1}{n\beta}\right) \quad (4.23)$$

where θ is measured from the radiating particle's direction.

1. Direct Monopole Cherenkov Emission

Magnetic monopoles radiate Cherenkov light directly [46] for $\beta_M > \frac{1}{n}$ with a Frank-Tamm spectrum (4.22), where Z^2 is replaced with $(\frac{1}{2\alpha})^2 \simeq 4700$ for minimally charged poles. Cherenkov light from an electric charge source is linearly polarized in the plane containing the path of the source and the direction of observation. However, the polarization of Cherenkov light from a magnetic charge will be rotated 90 degrees from that of an electric charge. This rotated polarization in principle offers a unique Cherenkov signature for monopoles [50].

The direct Cherenkov signature of a monopole leads to the best limits at present on the flux of relativistic monopoles of arbitrary mass. From the absence of a Cherenkov signal in deep water PMTs the Baikal Collaboration reports the limit $F_M \lesssim 6 \times 10^{-16}/\text{cm}^2/\text{s}/\text{sr}$ [47], while the absent signal in deep ice translates into the AMANDA limit $F_M \lesssim 1.6 \times 10^{-16}/\text{cm}^2/\text{s}/\text{sr}$ [48]. There is a comparable limit of $F_M \lesssim 4 \times 10^{-16}/\text{cm}^2/\text{s}/\text{sr}$ obtained by the MACRO collaboration using scintillators and streamer tubes [49]. Note that these limits are already slightly more restrictive than the Parker limit.

2. Coherent Radio-Wavelength Cherenkov Emission

In addition to the Cherenkov radiation from the bare monopole charge there is a contribution from each relativistic charged particle comprising the shower. Therefore, an estimation of the total power radiated in Cherenkov light requires a model for the monopole induced shower development.

The Radio Ice Cherenkov Experiment (RICE), if it were deployed, may offer the best chance for the detection of monopoles in a $\sim \text{km}^3$ scale detector. This expectation is based on two papers [51,52] for the RICE project which examine the viability of high energy neutrino studies in Antarctic ice. From these works one can approximate the sensitivity of the RICE array to the electromagnetic showers produced by a monopole.

Detailed Monte Carlo calculations of electromagnetic showers in ice [51] show that an electric charge excess, of about 20% the total shower size, accompanies the cascade ^{††}. Thus, we conclude that a monopole-induced shower will include an electron cloud of a total charge up to $10^4 e$.

The approximate lateral width of a monopole-induced cascade is given by the Molière radius which means the excess electric charge is confined roughly within a distance R_M . Cherenkov light of wavelength λ , for which $\lambda \gg R_M$, emitted by the monopole-induced shower will be radiated coherently and be strengthened by the Z^2 factor in eq. (4.22), where $Z^2 \simeq 10^8$.

^{††}The charge excess results from a number of processes involving the shower interacting with the medium. These include knock-on electrons, Compton scattering, and positron annihilation.

The monopole is highly penetrating and will traverse the full detector size without an appreciable loss of kinetic energy. Thus, the monopole signature is easily distinguished from a neutrino event (which is a localized shower that produces a Cherenkov cone, only detectable by a limited number of antennae that happen to lie within the cone). Timing can then be used to reconstruct the monopole path.

The monopole flux limits RICE could set are much stronger than those currently accessible (e.g., at Baikal, MACRO, or AMANDA [47,49,48]). A year of observation in the km^3 RICE detector without a candidate monopole event would set a flux limit $\lesssim 10^{-18} \text{ cm}^{-2} \text{ sec}^{-1} \text{ sr}^{-1}$.

C. Earth Tomography with Relativistic Monopoles

Direct knowledge about the composition and density of the earth's interior is lacking. Analysis of the seismic data is currently the best source of information about the earth's internal properties [53,54]. However, another potential probe would be the study of highly penetrating particles which could pass through the earth's interior and interact differently depending upon the composition and density of material traversed. With such a means it may be possible to directly measure the density profile of the earth's interior.^{§§}

Here we show that over a significant range of masses and initial energies, monopoles can pass through a large portion of the earth's interior and emerge with relativistic velocities. We present the results of a numerical calculation of relativistic monopoles passing through the earth, making use of the relevant energy loss expressions derived earlier and a simple model approximating the internal composition of the earth. We conclude that monopoles may initiate upgoing events in cosmic ray detectors.

1. Two Shell Earth Model

Dziewonski and Anderson [55] have developed the preliminary earth reference model (PREM) which is the standard earth model in use today. The PREM model consists of eight concentric shells of varying density and composition, but it is sufficient for our purposes to simplify this model to two shells, the mantle and the core***. Both shells are taken to be spherically symmetric. The mantle extends from the core out to the earth's surface at $R_{\oplus} = 6.371 \times 10^6 \text{ m}$ and has a mean mass density $\rho_{\text{mantle}} = 4.0 \frac{\text{g}}{\text{cm}^3}$. The core has a radius $R_{\text{core}} = 3.486 \times 10^6 \text{ m}$ and a mean mass density $\rho_{\text{core}} = 11.5 \frac{\text{g}}{\text{cm}^3}$. We take both shells to be of uniform composition. The chemical composition of the mantle (in weight) is approximated by SiO_2 (45.0%), Al_2O_3 (3.2%), FeO (15.7%), MgO (32.7%), and CaO (3.4%), and that of the core is approximated by Fe (96.0%) and Ni (4.0%) [56]. From these data we calculate the chemical composition (in percentage of *molecular type*) for the mantle as SiO_2 (40.0%), Al_2O_3 (1.67%), FeO (11.6%), MgO (43.6%), and CaO (3.23%), and for the core as Fe (96.2%) and Ni (3.8%).

^{§§}This idea has been exploited in neutrino physics as neutrinos are sufficiently weakly interacting to pass through the earth largely unimpeded for neutrino energies $\lesssim 10^{15} \text{ eV}$.

^{***}In principle, the eight shell model could be used in our calculations but it provides more detail than is needed here. The two shell approximation includes the gross features necessary to show tomography with monopoles.

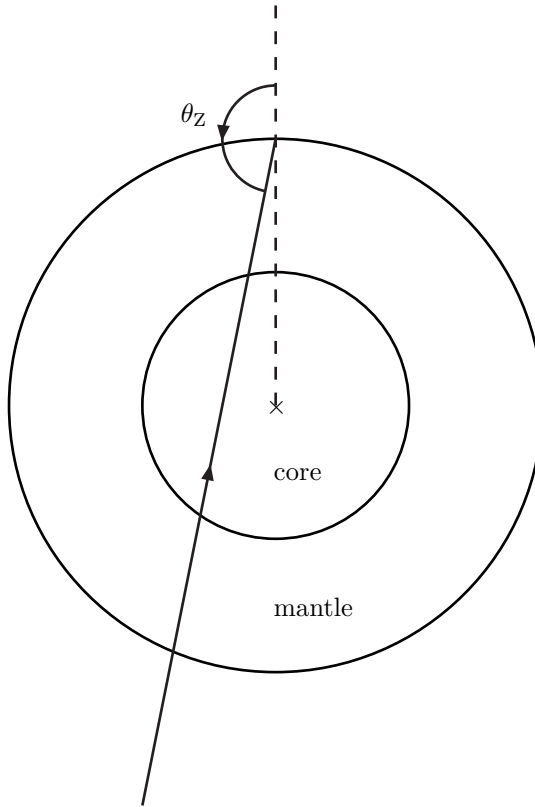


FIG. 5. A schematic representation of earth tomography with a highly penetrating particle. Monopole energy losses differ in passing through the core or mantle and so effect the energy spectrum of upcoming monopoles as a function of zenith angles, θ_Z . For a zenith angle $\theta_Z^{\text{core}} \simeq 147^\circ$ the upcoming particle will graze the edge of the core.

The terrestrial parameters relevant for the monopole stopping power must be determined. The electron number densities are

$$N_e = \begin{cases} 3.20 \times 10^{24} \text{ cm}^{-3} & (\text{core}) \\ 1.18 \times 10^{24} \text{ cm}^{-3} & (\text{mantle}) \end{cases}, \quad (4.24)$$

The energy loss processes are proportional to these number densities. Therefore, monopole tomography of the core is a possibility because $\frac{N_e^{(\text{core})}}{N_e^{(\text{mantle})}} \simeq 2.71$ and the monopole energy loss is boosted accordingly within the core.

The sundry parameters of the density effect must also be specified for the core and mantle of the earth. The density effect includes the following dimensionful parameters:

the plasma frequency [30]

$$\omega_p \simeq \begin{cases} 66.2 \text{ eV} = 3.36 \times 10^6 \text{ cm}^{-1} & (\text{core}) \\ 40.4 \text{ eV} = 2.05 \times 10^6 \text{ cm}^{-1} & (\text{mantle}) \end{cases}, \quad (4.25)$$

and the mean ionization potential [30]

$$I \simeq \begin{cases} 285 \text{ eV} & (\text{core}) \\ 172 \text{ eV} & (\text{mantle}) \end{cases}; \quad (4.26)$$

and various numbers in the Sternheimer and Peierls parameterization [31]:

$$C \equiv -2 \ln \left(\frac{I}{\omega_p} \right) - 1 \simeq \begin{cases} -3.92 & \text{(core)} \\ -3.90 & \text{(mantle)} \end{cases}, \quad (4.27)$$

$$a \equiv -\frac{C + 4.606X_0}{(X_1 - X_0)^3} \simeq \begin{cases} 0.137 & \text{(core)} \\ 0.136 & \text{(mantle)} \end{cases}, \quad (4.28)$$

where $X_0 = 0.2$ and $X_1 = 3.0$ for both the core and the mantle. The functional form [31] for $\delta(\gamma)$ in the core is

$$\delta^{\text{core}}(\gamma) \simeq \begin{cases} 0 & \gamma < 1.87 \\ -3.92 + \ln(\gamma^2 - 1) + 0.0297 [13.82 - \ln(\gamma^2 - 1)]^3 & 1.87 < \gamma < 1000 \\ -3.92 + \ln(\gamma^2 - 1) & 1000 < \gamma \end{cases}, \quad (4.29)$$

and in the mantle is

$$\delta^{\text{mantle}}(\gamma) \simeq \begin{cases} 0 & \gamma < 1.87 \\ -3.90 + \ln(\gamma^2 - 1) + 0.0295 [13.82 - \ln(\gamma^2 - 1)]^3 & 1.87 < \gamma < 1000 \\ -3.90 + \ln(\gamma^2 - 1) & 1000 < \gamma \end{cases}. \quad (4.30)$$

Lastly, the pair production and bremsstrahlung expressions are proportional to the mean nuclear charges

$$\bar{Z} \simeq \begin{cases} 26.1 & \text{(core)} \\ 10.8 & \text{(mantle)} \end{cases} \quad (4.31)$$

and pair production is dependent upon the mean atomic weights

$$\bar{A} \simeq \begin{cases} 56.1 & \text{(core)} \\ 21.7 & \text{(mantle)} \end{cases} \quad (4.32)$$

which are calculated from the chemical compositions given above.

2. Numerical Results

The variable we use for numerical integration is the lorentz boost factor $\gamma \equiv \frac{E}{M}$. We will integrate $\frac{d\gamma(x)}{dx} \equiv \frac{1}{M} \frac{dE(x)}{dx}$ to find $\gamma(x)$ at all points along the monopole trajectory. The input parameters are the monopole mass and initial boost factor (kinetic energy). The program calculates the final boost factor for the monopole after traversing the earth. For given input parameters, the calculation is performed at 200 different zenith angles, θ_Z . Depending on the zenith angle, the length and properties of the absorber will change (see Fig. 5), thereby allowing a determination of the earth's interior assuming we know the initial energy spectrum of the monopoles. The zenith angle for a trajectory tangent to the core boundary is

$$\theta_Z^{\text{core}} = \pi - \arcsin \left(\frac{R_{\text{core}}}{R_{\oplus}} \right) \simeq 147^\circ. \quad (4.33)$$

For each particular zenith angle, the function $\gamma_{\text{total}}(x)$ is calculated and the final value is stored. Thus, 200 final values of $\gamma_{\text{total}}(x)$ are stored along with their respective zenith angles. These are the data plotted in figures 6, 7, and

8. ^{†††}

Each figure has a fixed monopole mass and shows six plots representing six different initial kinetic energies. For zenith angle $\theta_Z \leq \frac{\pi}{2}$, these monopoles will have never passed through the earth and therefore retain the original kinetic energy attained from the large-scale magnetic fields. The energy dispersion of the incident monopoles can not be determined without detailed knowledge of the magnetic environment responsible for monopole acceleration. Presumably, the correct energy spectrum can be determined from the $\theta_Z \leq \frac{\pi}{2}$ data and compared with the $\theta_Z > \frac{\pi}{2}$ data to make a determination of the earth's interior.

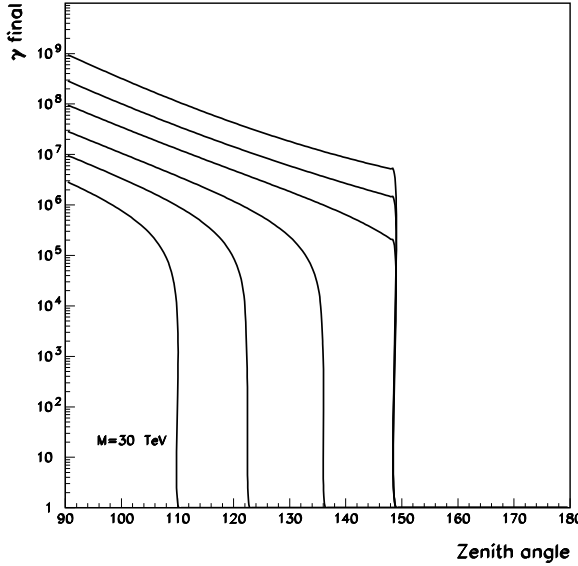


FIG. 6. The lightest allowed monopoles, $M = 30$ TeV, passing through the earth. The range of initial kinetic energies presented here is 9×10^{19} eV $< E_M < 3 \times 10^{22}$ eV.

^{†††}The angular resolution of earth tomography with monopoles is, in principle, limited by the multiple scattering of the monopole through small angles. However, the large monopole mass renders this angular uncertainty negligibly small.

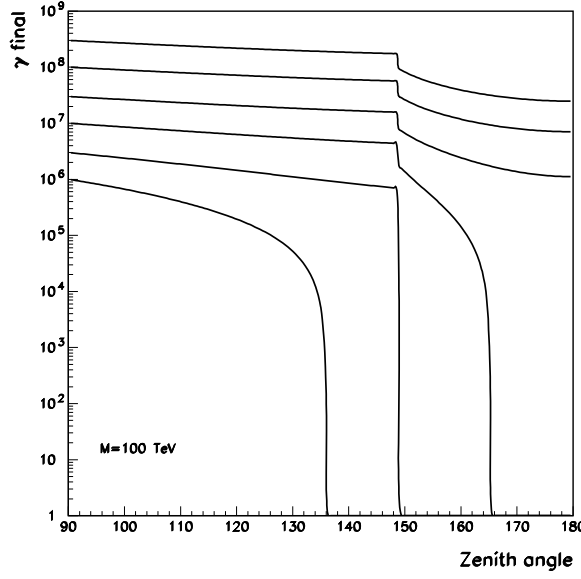


FIG. 7. $M = 100$ TeV monopoles passing through the earth. The range of initial kinetic energies presented here is $10^{20}\text{eV} < E_M < 3 \times 10^{22} \text{ eV}$.

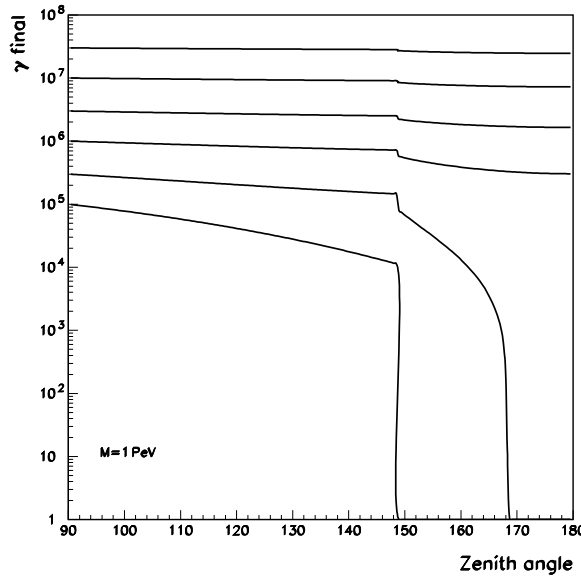


FIG. 8. $M = 1$ PeV monopoles passing through the earth. The range of initial kinetic energies presented here is $10^{20}\text{eV} < E_M < 3 \times 10^{22} \text{ eV}$.

3. Upgoing Monopole-Induced Shower

An upgoing monopole-induced shower will be created along the path followed by an upgoing monopole. When a monopole passes through a medium boundary, e.g., from the mantle into the atmosphere, the shower size will adjust to that sustainable by the shower regeneration rate of the new medium. (The atmospheric shower has about 30% fewer particles traveling along with the monopole than does shower in the mantle.) In Fly's Eye, OWL/Airwatch, or AUGER where shower development can be observed, this signature should be unique. X_{\max} will be at the earth's surface and the shower will be upward going, decreasing in strength until a fluorescence plateau is reached higher in the atmosphere.

4. Lunar Regolith Radio Emission

An attempt to infer the high energy neutrino flux incident on the moon by detecting the associated radio emission from showers in the lunar regolith has been undertaken recently [57]. Monopoles could also penetrate and emit sufficient power in radio-Cherenkov to become observable by the same means.

D. Monopole Fluorescence Signatures

A sensitive probe of high energy air shower development is the nitrogen fluorescence emitted by the atmosphere. In particular, the Fly's Eye and HiRes experiments have fruitfully pioneered this technique. Unfortunately, the nitrogen fluorescence technique does not appear promising for a monopole detection. The yield in nitrogen fluorescence is $\sim 0.5\%$ times the total energy in ionization of the atmosphere. Since $O(1)$ of the energy loss by all processes ends up in ionization of the atmosphere once the subshowers have ranged out, we need to evaluate the total stopping power to estimate the fluorescence yield. The total monopole-matter energy loss is the sum of the various processes summarized above:

$$\frac{dE_{\text{total}}}{dx} = \frac{dE_{\text{coll}}}{dx} + \frac{dE_{\text{pair}}}{dx} + \frac{dE_{\text{rad}}}{dx} + \frac{dE_{\text{had}}}{dx}. \quad (4.34)$$

For l -monopoles the electromagnetic energy loss dominates. However, in a thin absorber like the atmosphere l -monopole primaries are virtually undetectable via their fluorescence yield. ^{†††}

For light l -monopoles at extreme velocities

$$\frac{dE_{\text{total}}}{dx} \sim 2000 \frac{\text{TeV}}{\text{atm}} \left(\frac{Z}{7}\right) \left(\frac{100\text{TeV}}{M}\right) \left(\frac{\gamma}{10^8}\right) \ln\left(\frac{\gamma}{10^8}\right). \quad (4.35)$$

On the other hand q -monopoles, with color-magnetic charge, may have formed into baryonic-monopoles [19] and interact such that $\frac{dE_{\text{had}}}{dx}$ dominates the total energy loss. In section V a model for the baryonic monopole interaction

^{†††} For example, the energy threshold for Fly's Eye is $\sim 10^{17.3}$ eV [58] which renders the Eye blind to l -monopoles, with the possible exception of those with the smallest allowed mass at the greatest allowed kinetic energies. Consequently, we don't expect a measurable signature for these monopoles in air fluorescence experiments.

is developed. For baryonic monopoles a large energy transfer to the atmosphere may be natural. It seems possible to us that the energy transfer may be so large as to even mimic that of a proton.

V. BARYONIC-MONOPOLE AIR SHOWERS

The natural acceleration of monopoles to energies above the GZK cutoff at $E_{GZK} \sim 5 \times 10^{19}$ eV, and the allowed abundance of a monopole flux at the observed superGZK event rate motivates us to ask whether monopoles may contribute to the superGZK events. As a proof of principle, we here present a simple model of a baryonic-monopole interaction in air which produces a shower similar to that arising from a proton primary. To mimic a proton-induced shower the monopole must transfer nearly all of its energy to the shower in a very small distance. The large inertia of a massive monopole makes this impossible if the cross-section is typically strong, ~ 100 mb [60]. The cross-section we seek needs to be much stronger.

We model our arguments on [19] where three q -monopoles are confined by Z_3 strings of color-magnetic flux to form a color-singlet baryonic monopole. We further assume that 1) the cross-section for the interaction of the baryonic-monopole with a nucleus is geometric; in its unstretched state (before hitting the atmosphere) the monopole's cross-section is roughly hadronic, $\sigma_0 \sim \Lambda^{-2}$ (where $\Lambda \equiv \Lambda_{QCD}$); 2) each interaction between the monopole and an air nucleus transfers an $O(1)$ fraction of the exchanged energy into stretching the chromomagnetic strings of the monopole; 3) the chromomagnetic strings can only be broken with the formation of a monopole-antimonopole pair, a process which is highly suppressed and therefore ignored; other possible relaxation processes of the stretched string are assumed to be negligible;^{§§§} 4) the energy transfer per interaction is soft, $\frac{\Delta E}{E} \equiv \eta \sim \frac{\Lambda}{M}$.

The color-magnetic strings have a string tension $\mu \simeq \Lambda^2$. Therefore, when $O(1)$ of the energy transfer ($\gamma\Lambda$) stretches the color-magnetic strings (assumption 2), the length $L \sim \Lambda^{-1}$ increases by $\delta L = dE/\mu$, so that the fractional increase in length is $\delta L/L = \gamma$. Consequently, the geometrical cross-section grows $\propto \gamma$ after each interaction.

Already after the first interaction, the cross-section is sufficiently large to shrink the subsequent interaction length to a small fraction of the depth of first interaction. Thus, $O(1)$ of the monopole energy is transferred to the air nuclei over a short distance, just as in a hadron-initiated shower.

We can be more quantitative. From assumption 4) we infer that the total number of monopole-nucleus interactions required to transfer most of the monopole kinetic energy is roughly η^{-1} . From the above discussion, the geometrical cross-section after the first interaction will be

$$\sigma_1 \sim \frac{1 + \gamma}{\Lambda^2}. \quad (5.1)$$

The cross-section after n interactions is

$$\sigma_n \sim \frac{1 + \sum_{i=1}^n \gamma}{\Lambda^2} = \frac{1 + \gamma n(n+1)/2}{\Lambda^2}, \quad (5.2)$$

^{§§§} In the other extreme, it has been proposed [61] that the origin of the superGZK events is the gauge bosons radiated by cosmic monopole-string networks when the stretched strings relax.

where we have approximated $\gamma_n \sim (1 - \eta)^n \gamma \sim \gamma$. The mean-free-path, $\lambda \equiv 1/\sigma N$, after the n -th interaction is therefore

$$\lambda_n \sim \left(\frac{\Lambda^2}{N}\right)\left(\frac{2}{n^2\gamma}\right), n \geq 1, \quad (5.3)$$

where N is the density of nucleons, taken here to be a constant for simplicity of illustration. The total distance traveled between the first interaction and the $(\eta^{-1})^{\text{th}}$ interaction is

$$\Delta X \sim \sum_{n=1}^{\eta^{-1}} \lambda_n \quad (5.4)$$

which is, according to eq. (5.3),

$$\Delta X \sim \frac{2\Lambda^2}{N\gamma} \left(\sum_{n=1}^{\eta^{-1}} \frac{1}{n^2} \right). \quad (5.5)$$

The series is finite, and for $\eta^{-1} \gg 1$ is very nearly equal to $\zeta(2) = \pi^2/6$, giving

$$\Delta X \sim \left(\frac{\pi^2}{3}\right) \left(\frac{\Lambda^2}{\gamma N}\right), \quad (5.6)$$

in agreement with our earlier remark that the mfp for all interactions after the first are order $(1/\gamma)$ compared to the first. Thus the stretchable chromomagnetic strings of the baryonic monopole provide an example of a very massive monopole which nevertheless transfers $O(1)$ of its relativistic energy to an air shower over a very short distance. By construction, this baryonic monopole mimics the air-shower signature of a primary nucleon or nucleus.

VI. SUMMARY AND CONCLUSIONS

The challenge to seek a cosmic magnetic monopole flux below the Parker limit has now been met technologically. Therefore, renewed efforts to increase the search sensitivity are timely. Here we showed that the masses of monopoles whose fluxes are estimated to be in the observable range are significantly lighter than the heavy GUT scale. We also showed that such monopoles will be naturally accelerated by cosmic magnetic fields to relativistic energies. We then developed the possible and varied signatures by which a relativistic monopole flux may be identified.

ACKNOWLEDGEMENTS

We thank the Aspen Center for Physics for the environment that allowed this collaboration to begin, and A. Berera, A. Kusenko and G. Medina-Tanco for discussions. P. Biermann would like to thank Drs. H. Kang, P. Kronberg, C. Quigg and D. Ryu for extensive discussions on monopoles and magnetic fields in the cosmos. This work was supported in part by the U.S. Department of Energy grant no. DE-FG05-85ER40226, the Vanderbilt University Research Council, and NASA/Tennessee Space Grant Consortium.

- [1] T. W. Kibble, Phys. Rept. **67**, 183 (1980), and references therein.
- [2] E. N. Parker, Astrophys. J. **160**, 383 (1970); *ibid.* , **163**, 225 (1971); *ibid.* ,**166**, 295 (1971). Based on more speculative hypotheses, more stringent bounds have been proposed by M.S. Turner, E.N. Parker, and T. J. Bogdan, Phys. Rev. **D26**, 1296 (1982); Y. Rephaeli and M. S. Turner, Phys. Lett. **121B**, 115 (1983); F. Adams et al., Phys. Rev. Lett. **70**, 2511 (1993); M.J. Lewis, K. Freese, and G. Tarle, astro-ph/9911095.
- [3] N.A. Porter, Nuovo Cim. **16**, 958 (1960); E. Goto, Prog. Theo. Phys. **30**, 700 (1963).
- [4] T.W. Kephart and T.J. Weiler, Astropart. Phys. **4** 271 (1996); Nucl. Phys. (Proc. Suppl.) **51B**, 218 (1996).
- [5] G. 't Hooft, Nucl. Phys. **B79**, 276 (1974); A. Polyakov, JETP Lett. **20**, 194 (1974).
- [6] A. De Rujula, Nucl. Phys. **B435**, 257 (1995).
- [7] For a review and references see: M. B. Hindmarsh and T. W. Kibble, Rept. Prog. Phys. **58**, 477 (1995) [hep-ph/9411342].
- [8] S. F. King and Q. Shafi, Phys. Lett. **B422**, 135 (1998) [hep-ph/9711288].
- [9] D.K. Hong, J. Kim, J.E. Kim, and K.S. Soh, Phys. Rev. **D27**, 1651 (1983).
- [10] N. G. Deshpande, B. Dutta and E. Keith, Nucl. Phys. Proc. Suppl. **52A**, 172 (1997) [hep-ph/9607307]; Phys. Lett. **B388**, 605 (1996) [hep-ph/9605386]; Phys. Lett. **B384**, 116 (1996) [hep-ph/9604236].
- [11] P. H. Frampton and B. Lee, Phys. Rev. Lett. **64**, 619 (1990); P. H. Frampton and T. W. Kephart, Phys. Rev. **D42**, 3892 (1990).
- [12] M. Maldacena, Adv. Theor. Math. Phys. **D42**, 231 (1998).
- [13] P. H. Frampton, Phys. Rev. **D60**, 121901 (1999) [hep-th/9907051].
- [14] P. H. Frampton, Phys. Rev. **D60**, 085004 (1999) [hep-th/9905042]; P. H. Frampton and T. W. Kephart, [hep-th/9912028].
- [15] K. R. Dienes, E. Dudas, and T. Gherghetta, Phys. Lett. **B436**, 55 (1998) [hep-ph/9803466].
- [16] I.Antoniadis, N. Arkani-Hamed, S. Dimopoulos, and G. Dvali, Phys. Lett. **B436**, 257 (1998). [hep-ph/9804398]
- [17] C.L. Gardner and J.A. Harvey, Phys. Rev. Lett. **52**, 879 (1984).
- [18] T. Vachaspati, Phys. Rev. Lett. **76**, 188 (1996) [hep-ph/9509271]; H. Liu and T. Vachaspati, Phys. Rev. **D56**, 1300 (1997) [hep-th/9604138].
- [19] A. S. Goldhaber, Phys. Rept. **315**, 83 (1999) [hep-th/9905208].
- [20] E. Huguet and P. Peter, hep-ph/9901370.
- [21] D. Ryu, H. Kang, and P.L. Biermann, A&A. (in press) , [astro-ph/9803275].
- [22] K.-T. Kim et al., Nature **341**, 720 (1989).
- [23] R. Beck, Ann. Rev. Astron. & Astrophys. **34**, 155 (1996).

- [24] P.P. Kronberg et al., *Astrophys. J.* **246**, 751 (1981).
- [25] K.I. Kellermann and I.I.K Pauliny-Toth, *Ann. Rev. A&A* **19**, 373 (1981).
- [26] T.A. Enßlin, et al., *Astrophys. J.* **477**, 560 - 567 (1997).
- [27] R. Plaga, *Nature* **374**, 430 (1995).
- [28] M. Blagojevic and P. Senjanovic, *Phys. Rept.* **157**, 233 (1988); L. Gamberg and K. A. Milton, hep-ph/9910526.
- [29] G. Giacomelli, in: *Theory and Detection of Magnetic Monopoles in Gauge Theories*, ed. N. Craigie p.407 (Singapore: World Scientific Publishing Co., 1986).
- [30] S.P. Ahlen, *Rev. Mod. Phys.* **52**, 121 (1980).
- [31] R.M. Sternheimer, R.F. Peierls, *Phys. Rev. B* **3**, 3681 (1971).
- [32] H.A. Bethe and Heitler, *Proc. R. Soc. A* **146**, 83 (1934).
- [33] H.J. Bhabha, *Proc. Cambridge Philos. Soc.* **31**, 394 (1935).
- [34] S.D. Wick, Ph. D. Thesis, Vanderbilt University, 1999.
- [35] H. Cheng and T.T. Wu, *Expanding Protons: Scattering at High Energies* (Cambridge, Massachusetts: The MIT Press, 1987).
- [36] J. D. Jackson, *Classical Electrodynamics* (New York: John Wiley and Sons, 1975).
- [37] W. Heitler, *The Quantum Theory of Radiation*, (Oxford: Clarendon Press, 1954).
- [38] T.K. Gaisser, *Cosmic Rays and Particle Physics*, (Cambridge: Cambridge University Press, 1990); or A. M. Hillas, *Ann. Rev. Astron. Astrophys.* **22**, 425 (1984).
- [39] P. Sokolsky, *Introduction to Ultrahigh Energy Cosmic Ray Physics* (New York: Addison-Wesley Publishing Company, 1989).
- [40] S. Klein, LBNL-41167, [astro-ph/9712198].
- [41] L.D. Landau and I.J. Pomeranchuk, in *The Collected Papers of L.D. Landau*, (Oxford: Pergamon Press, 1965); A.B. Migdal, *Phys. Rev.* **103**, 1811 (1956).
- [42] R. Clay and P. Gerhardy, *Australian J. Phys.* **35**, 59 (1982).
- [43] Particle Data Group, *Phys. Rev. D* **50**, 1173 (1994).
- [44] B. Rossi, *High-Energy Particles* (New York: Prentice-Hall, 1952).
- [45] E. Fermi, *Phys. Rev.* **57**, 485 (1940).
- [46] D.R. Tompkins, *Phys. Rev.* **138**, B248 (1965).
- [47] V.A. Balkanov et al. (Baikal Collaboration), 26th International Cosmic Ray Conf. (ICRC99), Salt Lake City, UT, Aug.

17-25, 1999, paper H.E.5.3.04.

- [48] P. Niessen et al. (AMANDA Collaboration), 26th International Cosmic Ray Conf. (ICRC99), Salt Lake City, UT, Aug. 17-25, 1999, paper H.E.5.3.05.
- [49] B.C. Choudhary et al. (MACRO Collaboration), 26th International Cosmic Ray Conf. (ICRC99), Salt Lake City, UT, Aug. 17-25, 1999, paper H.E.5.3.02.
- [50] R. Hagstrom, *Phys. Rev. Lett.* **35**, 1677 (1975).
- [51] E. Zas, F. Halzen, and T. Stanev, *Phys. Rev. D* **45**, 362 (1992).
- [52] G.M. Frichter, J.P. Ralston, and D.W. McKay, *Phys. Rev. D* **53**, 1684 (1996).
- [53] T. Lay and T.C. Wallace, *Modern Global Seismology* (New York: Academic Press, 1995).
- [54] Properties of the Solid Earth, in *Rev. Geophys.* **33**, (1995); also at the URL: <http://earth.agu.org/revgeophys>.
- [55] A.M. Dziewonski and D.L. Anderson, *Phys. Earth Planet. Inter.* **25**, 297 (1981).
- [56] K.B. Krauskopf and D.K. Bird, *Introduction to Geochemistry* (New York: McGraw-Hill Publishers, 1995).
- [57] P. W. Gorham, K. M. Liewer, and C. J. Naudet, [astro-ph/9906504] and Proc. 26th International Cosmic Ray Conf. (ICRC99), Salt Lake City, UT, Aug. 17-25, 1999.
- [58] D. J. Bird et al., (Fly's Eye Collab.) *Astrophys. J.* **424**, 491 (1994); *ibid.* **441**, 144 (1995).
- [59] GR
- [60] R.N. Mohapatra and S. Nussinov, *Phys. Rev. D* **57**, 1940 (1998); in I.F.M. Albuquerque, G. Farrar, and E.W. Kolb, *Phys. Rev. D* **59**, 015021 (1999) it is noted that a baryon mass above 10 GeV produces a noticeably different shower profile, and a baryon mass above 50 GeV is so different as to be ruled out.
- [61] V. Berezinsky, X. Martin, and A. Vilenkin, *Phys. Rev. D* **56**, 2024 (1997); V. Berezinsky and A. Vilenkin, *Phys. Rev. Lett.* **79**, 5202 (1997); V. Berezinsky, P. Blasi, and A. Vilenkin, astro-ph/9803271 and *Phys. Rev. D*, to appear.